

A Diruthenium Catalyst for Selective, Intramolecular Allylic C–H Amination: Reaction Development and Mechanistic Insight Gained through Experiment and Theory

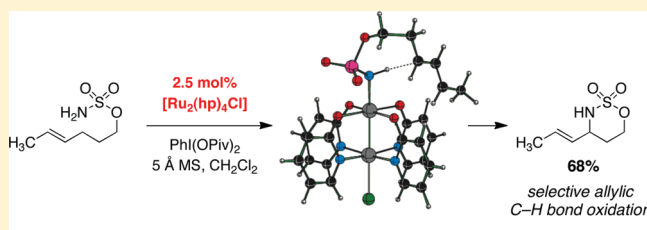
Mark Edwin Harvey,[†] Djamaladdin G. Musaev,^{*,‡} and J. Du Bois^{*,†}

[†]Department of Chemistry, Stanford University, Stanford, California 94305-5080, United States

[‡]Emerson Center for Scientific Computation, Emory University, Atlanta, Georgia 30322-0001, United States

 Supporting Information

ABSTRACT: The mixed-valent paddlewheel complex tetrakis-(2-oxyppyridinato)diruthenium(II,III) chloride, $[\text{Ru}_2(\text{hp})_4\text{Cl}]$, catalyzes intramolecular allylic C–H amination with bis-(homoallylic) sulfamate esters. These results stand in marked contrast to reactions performed with dirhodium catalysts, which favor aziridine products. The following discussion constitutes the first report of C–H amination using complexes such as $[\text{Ru}_2(\text{hp})_4\text{Cl}]$ and related diruthenium adducts. Computational and experimental studies implicate a mechanism for $[\text{Ru}_2(\text{hp})_4\text{Cl}]$ -promoted C–H amination involving hydrogen-atom abstraction/radical recombination and the intermediacy of a discrete, albeit short-lived, diradical species. The collective data offer a coherent model for understanding the preference of this catalyst to oxidize allylic (and benzylic) C–H bonds.



INTRODUCTION

Diruthenium Catalysts. Tetra-bridged dirhodium(II) complexes (e.g., $[\text{Rh}_2(\text{OAc})_4]$) hold a certain distinction among metal catalysts that mediate selective C–H and π -bond functionalization. These systems appear to be uniquely suited for stabilizing reactive carbene and nitrene intermediates and can bias the formation of products in a controlled and highly predictive manner. Substitution of the ligand architecture is possible with a number of bridging ligand types, such as carboxylates, amidates, and ortho-metalated arylphosphines. The majority of these complexes effectively engage diazoalkane substrates to promote C–C bond formation or olefin cyclopropanation; the ability to choose among such disparate catalyst systems makes possible reagent-level control of reaction selectivity.¹ For dirhodium-mediated C–H amination, the range of ligand–metal architectures that promote this transformation is decidedly smaller, limited primarily to tetracarboxylate-based designs. The facility with which the dirhodium core oxidizes under the conditions of nitrenoid formation appears to be, at least in part, responsible for the inability to conduct amination reactions with a more diverse set of dirhodium catalysts. Such is the case with rhodium tetraamidates (e.g., the caprolactamate adduct $[\text{Rh}_2(\text{cap})_4]$; $E_{1/2} = 11$ mV vs SCE), which oxidize immediately in the presence of iodine(III) reagents to catalytically inactive forms.^{2,3}

For some time, we have sought new catalyst systems for C–H amination that would provide greater flexibility in ligand design. In principle, judicious modification of the ligand sphere could enable reagent-controlled chemo- and/or stereoselective C–N bond formation. In addition to rhodium, a variety of metal

complexes, including those derived from copper, manganese, iron, cobalt, ruthenium, silver, and gold, can effect C–H amination.^{4–11} None of these systems, however, appears to match the universal performance of dirhodium tetracarboxylate catalysts for both intra- and intermolecular C–H bond oxidation. Studies in our lab to identify mononuclear metal complexes [e.g., Ru(II) –arene adducts] that promote C–H amination have met with minimal success. By contrast, Che and Blakey have described in independent accounts the impressive performance of porphyrin- and pybox-derived Ru(II) complexes, respectively, for C–H amination reactions.⁹ These reports have inspired our continued examination of ruthenium complexes as N-atom-transfer catalysts.

Synthetic and spectroscopic studies of mixed-valent diruthenium paddlewheels find extensive literature discourse.¹² Despite a rich history of investigation, these complexes have seldom found use in catalytic reaction development (examples include sulfide oxygenation and amine and alcohol oxidation).¹³ Germane to our interests, recent reports by Berry describe the preparation and characterization of a unique diruthenium nitride complex capable of stoichiometric aryl C–H amination of a ligand residue.¹⁴ For our purposes, one evident advantage of these mixed-valent ruthenium dimers for catalytic atom-transfer processes is the high one-electron oxidation potentials for both tetracarboxylate and tetraamidate complexes.¹⁵ Accordingly, diruthenium catalysts derived from a number of bridging ligand

Received: April 19, 2011

Published: October 07, 2011

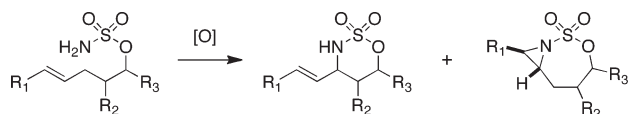


Figure 1. Controlling product selectivity through catalyst design.

types should be stable against the oxidizing conditions of the amination reaction.

The following report highlights the unique properties of diruthenium complexes for C–H amination. One catalyst in particular, tetrakis(2-oxyppyridinato)diruthenium(II,III) chloride, $[\text{Ru}_2(\text{hp})_4\text{Cl}]$, has proven markedly effective at favoring allylic C–H amination over competing aziridination of unsaturated sulfamate esters (Figure 1).¹⁶ The bias displayed by this catalyst for allylic oxidation is distinguished from analogous reactions with dirhodium systems and rationalized mechanistically through experimental and computational analysis, as described below.

Chemoselective C–H Amination. Selective oxidation of allylic C–H bonds in unsaturated substrates presents a considerable challenge in methods development research. The design of palladium-based catalytic processes, which operate through C–H activation and the intermediacy of π -allyl species, offers an elegant solution to this problem, enabling access to both allylic alcohol and amine derivatives.¹⁷ For reactions that proceed via heteroatom-transfer mechanisms, oxidation of unsaturated substrates typically results in mixtures of C–H- and π -bond-functionalized products, generally favoring the latter. Notable exceptions can be found for intramolecular reactions of sulfamate esters with select dirhodium and mononuclear ruthenium catalysts.^{9,18} In these cases, allylic amine derivatives are obtained as the predominant products. A related example of intermolecular allylic amination in which the specific combination of dirhodium catalyst and nitrogen source (sulfonimidamides) appears to be critical for achieving selective C–H bond oxidation has also been demonstrated.¹⁹

To expand the scope of C–H amination technologies for fine-chemicals synthesis, we desire catalysts that afford reagent control over chemoselectivity. Our recent explorations involving $[\text{Ru}_2(\text{hp})_4\text{Cl}]$ have shown the proclivity of this catalyst to furnish products of selective allylic amination. This reactivity profile appears to be general with a range of bis(homoallylic) sulfamate esters.

RESULTS AND DISCUSSION

Preparation of Diruthenium Complexes. The preparation of $[\text{Ru}_2(\text{OAc})_4\text{Cl}]$ was first described by Stephenson and Wilkinson²⁰ and proceeds by refluxing an acetic acid solution containing $\text{RuCl}_3 \cdot x\text{H}_2\text{O}$, acetic anhydride, and LiCl. The reaction can be followed by visual inspection, as a burgundy solid slowly precipitates from the red-black solution. The acetate complex provides a convenient starting material for accessing all other analogous diruthenium adducts.

We have prepared a number of structurally disparate diruthenium complexes by ligand metathesis with $[\text{Ru}_2(\text{OAc})_4\text{Cl}]$. These reactions are performed in refluxing $\text{C}_6\text{H}_5\text{Cl}$, from which the liberated acetic acid is distilled. Typically, the desired complex is obtained as a brick-red solid that precipitates from the $\text{C}_6\text{H}_5\text{Cl}$ solution upon cooling. The paramagnetic nature of this material renders characterization by NMR impractical; however,

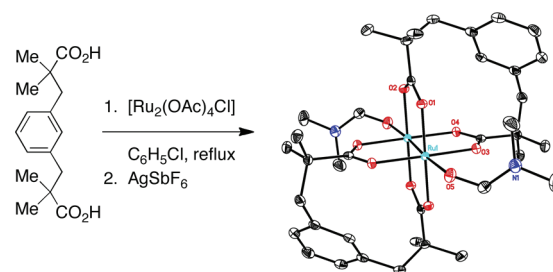


Figure 2. ORTEP diagram of $[\text{Ru}_2(\text{esp})_2\text{SbF}_6] \cdot 2\text{DMF}$; the SbF_6^- counterion and H atoms are not pictured. Ru–Ru bond distance = 2.267 Å. Single crystals were grown by vapor-phase diffusion of toluene into a DMF solution.

the ligand-exchange process can be followed by mass spectrometry and is generally quantitative given the appropriate reaction time. It is possible to exchange the axially bound chloride ligand with a noncoordinating anion by treatment of the complex with a silver salt.

The notable performance of $[\text{Rh}_2(\text{esp})_2]$ for catalytic C–H amination reactions motivated our interest in preparing the analogous diruthenium adduct. The dicarboxylic acid α, α', α' -tetramethyl-1,3-benzenedipropionic acid (H_2esp), when heated with $[\text{Ru}_2(\text{OAc})_4\text{Cl}]$ in $\text{C}_6\text{H}_5\text{Cl}$, affords $[\text{Ru}_2(\text{esp})_2\text{Cl}]$ as a clay-red powder. Treatment of this material with AgSbF_6 yields the Cl-exchanged product (orange), which was crystallized by vapor-phase diffusion of toluene into an *N,N*-dimethylformamide (DMF) solution to give single crystals suitable for X-ray diffraction. The ORTEP diagram ($C2/c$ space group) reflects a molecular structure having C_{2h} symmetry with a measured Ru–Ru bond distance of 2.27 Å (Figure 2). Such a value is in accordance with a formal Ru–Ru bond order of 2.5. By contrast, the metal–metal bond length in $[\text{Rh}_2(\text{esp})_2]$ is slightly longer at 2.38 Å, consistent with a Rh–Rh single bond. Other metrical parameters are largely conserved between the dirhodium- and diruthenium-esp complexes; for example, the metal–ligand Ru–O distances (~ 2.02 Å) are nominally shorter than their rhodium counterparts (~ 2.04 Å). In the structure of $[\text{Ru}_2(\text{esp})_2\text{SbF}_6] \cdot 2\text{DMF}$, a DMF molecule is bound axially to each ruthenium center.

Both the chloride and hexafluoroantimonate diruthenium-esp complexes are indefinitely stable in air under ambient conditions. It should be noted that the structure of $[\text{Ru}_2(\text{esp})_2\text{Cl}] \cdot \text{H}_2\text{O}$ has been disclosed previously and that this complex has been shown to catalyze sulfide oxygenation with *t*-BuOOH.^{13a}

To assess the performance of alternative, noncarboxylate-derived diruthenium catalysts for C–H amination, we performed metathesis reactions with $[\text{Ru}_2(\text{OAc})_4\text{Cl}]$ and both amide and oxyppyridine ligands. This report will focus principally on the complex derived from 2-hydroxyppyridine, given its unique reactivity with unsaturated sulfamates. The synthesis of $[\text{Ru}_2(\text{hp})_4\text{Cl}]$ proceeded in a manner analogous to that of $[\text{Ru}_2(\text{esp})_2\text{Cl}]$, and the burgundy complex was isolated in 90% yield by filtration of the reaction mixture. X-ray crystallographic analysis of a single crystal of this product grown from DMF rendered the ORTEP diagram shown in Figure 3. The pseudo- C_{4v} symmetric hp complex crystallizes in the $C2/c$ space group with a measured Ru–Ru bond length of 2.29 Å. The four 2-oxyppyridinate groups bind the diruthenium core in an all-polar arrangement (4,0 geometry) in which the four pyridine nitrogens coordinate the same ruthenium center. The chloride ligand resides in a position

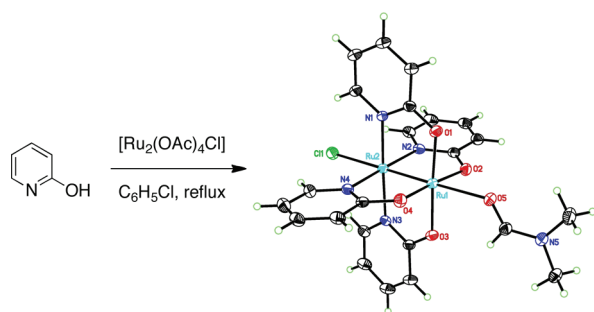


Figure 3. ORTEP diagram of $[\text{Ru}_2(\text{hp})_4\text{Cl}] \cdot \text{DMF}$. Ru1–Ru2 bond distance = 2.295 Å.

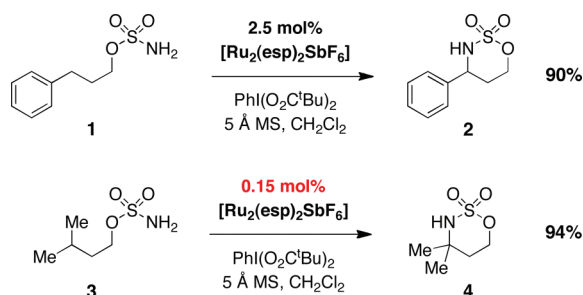


Figure 4. Intramolecular amination reactions on benzylic and tertiary centers efficiently catalyzed by $[\text{Ru}_2(\text{esp})_2\text{SbF}_6]$.

trans to the Ru–Ru bond on the more sterically hindered Ru2 center. A single DMF molecule, bound through oxygen, fills the remaining coordination site of Ru1. The synthesis and crystallographic characterization of a related oxypyridinate ruthenium dimer has appeared previously.²¹

Catalytic C–H Amination Reactions. Initial attempts to effect oxidation of 3-phenylpropyl sulfamate ester (**1**) using $[\text{Ru}_2(\text{OAc})_4\text{Cl}]$ and $\text{PhI}(\text{OAc})_2$ provided exceptionally low yields of heterocycle **2**, a result ascribed to the markedly insoluble nature of the ruthenium complex in all of the solvents tested. The corresponding SbF_6^- derivative fared only slightly better as a catalyst for this reaction. By contrast, use of either esp complex $[\text{Ru}_2(\text{esp})_2\text{Cl}]$ or $[\text{Ru}_2(\text{esp})_2\text{SbF}_6]$ resulted in improved levels of product conversion, the latter exhibiting clear superiority. When used in combination with the more soluble oxidant $\text{PhI}(\text{O}_2\text{C}^t\text{Bu})_2$ and 5 Å molecular sieves, $[\text{Ru}_2(\text{esp})_2\text{SbF}_6]$ mediates efficient intramolecular amination of C–H bonds, rivaling the established performance of its rhodium congener (Figure 4). The oxidative cyclization of isoamyl sulfamate (**3**) with only 0.15 mol % $[\text{Ru}_2(\text{esp})_2\text{SbF}_6]$ is exemplary in this regard.

Explorations into the reactivity and substrate scope of $[\text{Ru}_2(\text{esp})_2\text{SbF}_6]$ revealed that this and related diruthenium adducts function optimally in refluxing CH_2Cl_2 . The addition of MgO , a useful additive for dirhodium-promoted C–H amination, is deleterious to the reaction with $[\text{Ru}_2(\text{esp})_2\text{SbF}_6]$. Other soluble organic bases and salts such as Al_2O_3 are similarly ineffectual. On the other hand, ground and activated 5 Å molecular sieves significantly enhance the substrate conversion (3 and 4 Å sieves give analogous results). Control experiments indicated that small amounts of H_2O , in addition to other polar, coordinating solvents such as CH_3OH , dioxane, DMF, and isopropyl acetate, inhibit catalyst turnover. Thus, the role of

Table 1. Bis(homoallylic) Sulfamate Ester Cyclization Catalyzed by Several Ruthenium and Rhodium Complexes

entry ^a	catalyst	I/A ^b	entry	catalyst	I/A ^b
1	$[\text{Ru}_2(\text{OAc})_4\text{Cl}]$	1:3 ^c	6	$[\text{Ru}_2(\text{hp})_4\text{SbF}_6]$	8:1
2	$[\text{Ru}_2(\text{OAc})_4\text{SbF}_6]$	1:3 ^c	7	$[\text{Rh}_2(\text{OAc})_4]$	2:1
3	$[\text{Ru}_2(\text{esp})_2\text{Cl}]$	1:2 ^c	8	$[\text{Rh}_2(\text{O}_2\text{CCPh}_3)_4]$	1:5
4	$[\text{Ru}_2(\text{esp})_2\text{SbF}_6]$	1:5	9	$[\text{Rh}_2(\text{esp})_2]$	1:1
5	$[\text{Ru}_2(\text{hp})_4\text{Cl}]$	8:1 (68) ^d	10	$[\text{Rh}_2(\text{hp})_4]$	3:1 ^c

^a Reactions were performed at 40 °C using 1.4 equiv of $\text{PhI}(\text{O}_2\text{C}^t\text{Bu})_2$, powdered 5 Å molecular sieves, and 2.5 mol % catalyst. ^b Product ratios were estimated by integration of the ^1H NMR spectrum of the unpurified reaction mixture. ^c Less than 20% conversion to product. ^d Isolated yield following chromatographic purification.

cat.	A	B	A	B	C	A	B	C	
I	1.0	7.0	1.3	1.0	1.8	0.2	1.0	0.5	$[\text{Rh}_2(\text{esp})_2]$
II	1.0	6.0	0.3	1.0	1.6	–	1.0	1.5	$[\text{Ru}_2(\text{esp})_2\text{SbF}_6]$
III	1.0	1.2	0.7	1.0	0.4	0.6	1.0	1.0	$[\text{Rh}_2(\text{hp})_4]$
IV	1.5	1.0	0.2	1.0	–	0.3	1.0	–	$[\text{Ru}_2(\text{hp})_4\text{Cl}]$

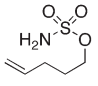
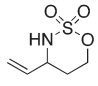
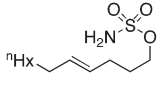
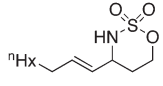
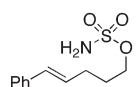
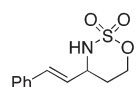
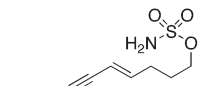
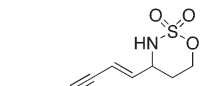
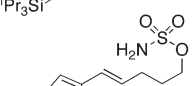
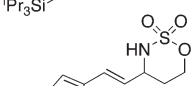
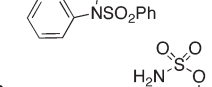
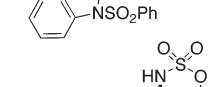
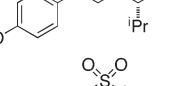
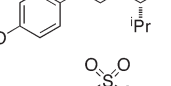
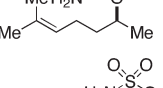
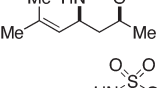
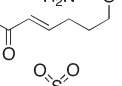
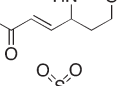
Figure 5. Oxidation of differentially substituted sulfamate esters catalyzed by selected rhodium and ruthenium complexes.

molecular sieves in this reaction is presumably to scavenge adventitious H_2O .

While diruthenium complexes derived from substituted carboxylate, amide, and pyridinate groups all show some degree of activity for the oxidation of *trans*-4-hexenyl sulfamate, only the tetra-2-oxypyridinate ruthenium dimer $[\text{Ru}_2(\text{hp})_4\text{Cl}]$ rivals the catalytic efficiency of $[\text{Ru}_2(\text{esp})_2\text{SbF}_6]$ (Table 1). The hp system, however, displays a greater bias toward allylic oxidation than any other catalyst we have examined to date and gives the oxathiazinane heterocycle in 68% yield.²² Interestingly, the analogous $[\text{Rh}_2(\text{hp})_4]$ complex demonstrates a similar predilection for C–H amination over aziridination, although the general performance of this catalyst is quite poor. The ineffectiveness of this dirhodium complex at promoting amination is likely due to both poor solubility and the facility by which it is oxidized under the amination conditions.

A series of amination reactions using bifunctional substrates enabled an assessment of chemoselectivity differences between diruthenium and dirhodium catalysts. Reactions with the three substrates shown in Figure 5 were performed with $\text{PhI}(\text{O}_2\text{C}^t\text{Bu})_2$ and 5 Å molecular sieves; product conversions were quantitative in all cases except when $[\text{Rh}_2(\text{hp})_4]$ was employed. While the variations in the product profiles are admittedly small, the data clearly reflect the preference of $[\text{Ru}_2(\text{hp})_4\text{Cl}]$ to oxidize allylic

Table 2. Allylic Amine Formation Catalyzed by $[\text{Ru}_2(\text{hp})_4\text{Cl}]$

entry ^a	substrate	major product	I/A ^b	yield
1			2:1	35
2			12:1	73
3			8:1	66
4			20:1	71
5			20:1	59
6			20:1	63 ^c
7			20:1	74 ^d
8			20:1	25
9			20:1	75 ^e

^a All reactions were performed with 2.5 mol % $[\text{Ru}_2(\text{hp})_4\text{Cl}]$, 1.4 equiv of $\text{PhI}(\text{O}_2\text{C}^t\text{Bu})_2$, and powdered 5 Å molecular sieves in CH_2Cl_2 at 40 °C. ^b Product ratios were estimated by integration of the ^1H NMR spectrum of the unpurified reaction mixture. ^c Product obtained as a 12:1 mixture of diastereomers; major product shown. ^d Product obtained as a 2:1 mixture of diastereomers; major product shown. ^e Product obtained as a > 20:1 mixture of diastereomers.

and benzylic C–H bonds over both π bonds and tertiary centers. Notably, in the two examples involving this catalyst and an unsaturated sulfamate ester, the aziridine product was not detected. These selectivity trends diverge unmistakably from data recorded for $[\text{Rh}_2(\text{esp})_2]$ and other tetracarboxylate rhodium dimers. We believe that the identification of $[\text{Ru}_2(\text{hp})_4\text{Cl}]$ represents an important breakthrough for C–H amination technology, affording us the ability to influence reaction chemoselectivity in a single substrate with a simple choice of catalyst.

The utility of $[\text{Ru}_2(\text{hp})_4\text{Cl}]$ was explored against a collection of structurally disparate substrates. The reaction afforded in all cases the oxathiazinane heterocycle as the major (or exclusive) product of oxidation (Table 2). The reactions were easily conducted without the need for rigorously dried solvent or oxygen-free conditions and reached completion in less than 24 h. The process appears to be compatible with a number of common functional groups and proceeds efficiently with di- and trisubstituted alkene

	Expt	Calcd
$\text{Ru}^1\text{--Ru}^2$	2.295	2.327
$\text{Ru}^1\text{--O}$	1.990	2.008
$\text{Ru}^2\text{--N}$	2.107	2.159
$\text{Ru}^2\text{--Cl}$	2.558	2.525

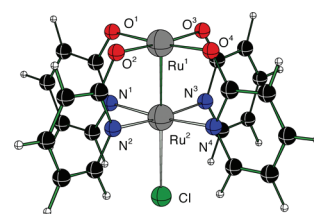


Figure 6. Comparison of selected bond distances in $[\text{Ru}_2(\text{hp})_4\text{Cl}]$ from computational and crystallographic data.

derivatives. The low product yield and poor chemoselectivity afforded by 4-pentenyl sulfamate (entry 1) may reflect the instability of an intermediate radical (see below). As noted previously for the dirhodium-catalyzed process, electron-withdrawing groups proximal to the desired site of oxidation tend to decrease the overall reaction performance. Chiral substrates afford oxathiazinane products with modest levels of diastereocontrol (12:1 and 2:1 dr for entries 6 and 7, respectively).²³ The preferred sense of induction in these reactions can be rationalized through a putative chairlike transition structure.²⁴

The evident bias of $[\text{Ru}_2(\text{hp})_4\text{Cl}]$ for allylic C–H bond oxidation over the range of substrates depicted in Table 2 encouraged a deeper examination of the reaction mechanism, the results of which are discussed below.

Mechanistic Analysis: Computational. *General.* There exist two general and limiting mechanistic scenarios for C–H amination by a metal–nitrene complex. The first operates by way of a closed-shell singlet nitrene, resulting in a concerted (likely asynchronous) oxidative process. An alternative pathway proceeds through a stepwise mechanism involving initial H-atom abstraction followed by diradical recombination. A substantial body of experimental and computational evidence on dirhodium-mediated C–H insertion implicates a concerted process.²⁵ By contrast, related mechanistic studies on monomeric ruthenium amination catalysts (e.g., $[\text{Ru}(\text{TPP})\text{CO}]$) support a stepwise oxidative event.²⁶ In an effort to understand the operative mechanism for diruthenium-catalyzed amination, a comprehensive theoretical analysis of the reaction coordinate for both allylic oxidation and π -bond aziridination was undertaken.

In the following section, relevant energies (298.15 K, 1 atm) are tabulated as $\Delta H(\Delta G)[\Delta G_s]$ for gas-phase enthalpy, gas-phase Gibbs free energy, and solvated Gibbs free energy, the last of which was estimated as $\Delta G_s = \Delta G_{\text{solv}}(\text{PCM-calculated}) + [\Delta E - \Delta G]_{\text{gas}}$. Cartesian coordinates for all of the B3LYP/LANL2DZ-optimized structures are presented in Table S2 in the Supporting Information.²⁷ High-spin states were calculated for all reported structures; computed molecular orbitals were then used to determine both open- and closed-shell low and intermediate spin states.

Initial calculations were able to recapitulate to within close approximation the crystallographic data obtained for $[\text{Ru}_2(\text{hp})_4\text{Cl}]$ and indicated that the most stable isomer should maintain a (4,0) ligand geometry with chloride bound to the more sterically congested ruthenium center (Figure 6). The ground electronic state of $[\text{Ru}_2(\text{hp})_4\text{Cl}]$ is a ^4A state with three unpaired spins, in agreement with magnetic susceptibility measurements on this and analogous diruthenium complexes.¹² The open-shell ^2A state is 8.4(8.7)[17.9] kcal/mol higher in energy. The spin-paired “closed-shell” doublet ($\langle S^2 \rangle = 0.76$) is higher in energy by 13.1(13.9)[21.2] kcal/mol and was not further examined.

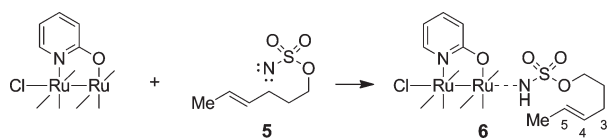


Figure 7. Model reaction for evaluating the putative nitrenoid oxidant.

Mulliken spin-density analysis of $[\text{Ru}_2(\text{hp})_4\text{Cl}]$ in the ^4A ground state indicated that 1.71 unpaired α -spins reside on Ru^1 , whereas almost one full α -spin is localized on Ru^2 . The Cl center and bridging N and O atoms of the oxypyridinate (hp) ligands bear additional small amounts of unpaired α -spin. The number of unpaired spins on Ru^2 does not change in the ^2A state, while that on Ru^1 is reduced from 1.71 to 0.40. In the ^2A state, both the N and O atoms of the hp ligands support small amounts of unpaired β -spins. This spin distribution, along with the calculated $\langle S^2 \rangle$ value of 1.76, confirms the antiferromagnetically coupled nature of the open-shell doublet of $[\text{Ru}_2(\text{hp})_4\text{Cl}]$. Table S1 in the Supporting Information (SI) summarizes these data.

Having validated the choice of basis set and functional, we evaluated the structure of the putative $[\text{Ru}_2(\text{hp})_4\text{Cl}]$ –nitrene complex **6**. A general scheme for performing this analysis combines $[\text{Ru}_2(\text{hp})_4\text{Cl}]$ with neutral nitrene fragment **5** (Figure 7). Table S1 in the Supporting Information contains calculated spin densities of relevant atoms for intermediates, transition states, and products in both the quartet and open-shell doublet states for the reaction between $[\text{Ru}_2(\text{hp})_4\text{Cl}]$ and *trans*-4-hexenyloxysulfonylnitrene (**5**).

The ground electronic state of alkoxy sulfonylnitrene **5** is a triplet with two unpaired electrons occupying degenerate orbitals on the N center. An open-shell singlet state for **5** ($\langle S^2 \rangle = 1.01$) lies 11.5(12.4)[11.5] kcal/mol higher in energy. The closed-shell singlet state of this free nitrene ($\langle S^2 \rangle = 0.00$) appears to be 18.6(19.9)[18.5] kcal/mol higher than the triplet state and was not evaluated further.²⁸

Combining the ^4A and ^2A states of $[\text{Ru}_2(\text{hp})_4\text{Cl}]$ with triplet and singlet forms of **5** generates Ru–nitrene complex **6** in three possible electronic states: doublet, quartet, and sextet. Our calculations suggest that **6** is a ground-state doublet with 0.82 unpaired α -spins located on Ru^2 (Figure 8). The Ru^1 and sulfonyl nitrogen (N^5) centers bear small contributions of 0.09 α -spin and 0.07 β -spin, respectively. This spin distribution is in accord with a Ru–nitrene double bond in the doublet state of complex **6**. The quartet state of **6** resides 9.8(6.7)[5.4] kcal/mol higher in energy than the doublet state; the calculated spin densities (0.92, 0.96, and 0.64 α -spins in Ru^1 , Ru^2 , and N^5 , respectively) indicate that Ru^1 – N^5 is a single bond in quartet **6**. The sextet state energy lies significantly above those calculated for the ^2A and ^4A states, so further discussion of this state has been omitted.

The estimated Ru^1 – N^5 bond distances for the ^2A and ^4A states of **6** are consistent with the predicted bond orders. The short Ru^1 – N^5 distance of 1.789 Å in doublet **6** is characteristic of doubly bonded Ru–N. In the quartet form, the predicted Ru^1 – N^5 distance of 1.904 Å more closely resembles a metal–nitrogen single bond. Association of the nitrene to Ru^1 elongates the Ru^1 – Ru^2 distance from 2.327 to 2.559 and 2.508 Å for doublet and quartet states of **6**, respectively. The consequence of this bond lengthening is a decrease in the bonding overlap between the two ruthenium centers. Since the doublet and quartet electronic states of the metal–nitrene complex are

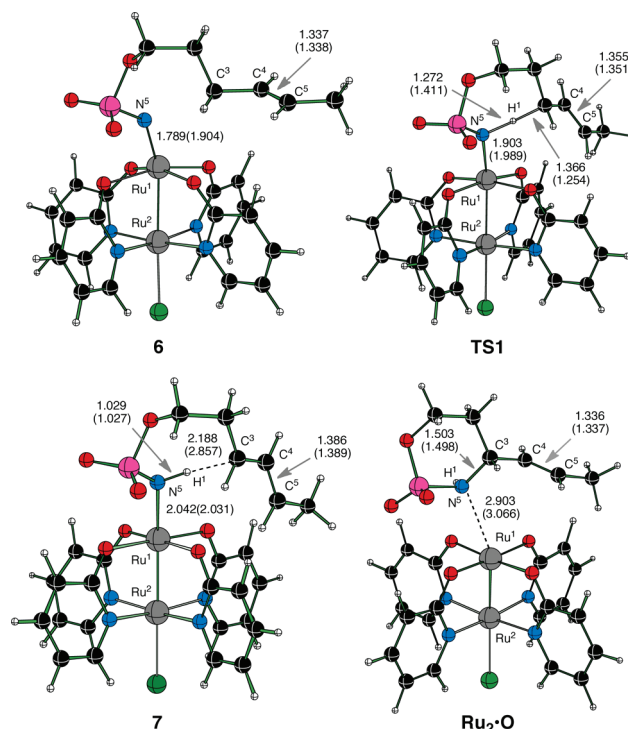


Figure 8. Calculated structures for the $[\text{Ru}_2(\text{hp})_4\text{Cl}]$ -catalyzed allylic amination pathway: metal-bound nitrenoid **6**, transition state **TS1**, diradical intermediate **7**, and metal-bound oxathiazinane adduct $\text{Ru}_2\cdot\text{O}$. Numerical values represent selected bond lengths (in Å) for doublet electronic states. Corresponding values for quartet electronic states are in parentheses.

energetically similar, both were studied for all possible transition states, intermediates, and products of the reaction (for both C–H amination and olefin aziridination). The computed energies of these structures are reported relative to the corresponding doublet and quartet states of **6**, unless otherwise stated.

Allylic C–H Amination Pathway. Intramolecular allylic amine formation from **6** occurs via insertion of a ruthenium-bound nitrene into the allylic C^3 –H bond. The transition state **TS1** associated with this process (starting from the ground-state doublet form of **6**) is shown in Figure 8; the analogous quartet TS is predicted to be only 1.8(1.1)[1.0] kcal/mol higher in energy. The general pathway for this reaction starting from nitrenoid intermediate **6** is given by $\mathbf{6} \rightarrow \mathbf{TS1} \rightarrow \mathbf{7} \rightarrow \mathbf{Ru}_2\cdot\text{O}$. In the ^2A TS, 0.68 unpaired α -spin is located on the distal Ru^2 center, while other atoms bear insignificant spin densities (see Table S1 in the Supporting Information). In the ^4A TS, however, the Ru^1 , Ru^2 , N^5 , C^3 , and C^5 centers harbor significant α -spin densities (0.97, 0.76, 0.48, 0.27, and 0.23, respectively). These data intimate that the quartet state of **TS1** may represent a proton-coupled electron-transfer (PCET) process. Calculations on the ^2A state for **TS1** suggest insignificant spin contributions at both the C^3 and C^5 centers.

Calculated bond distances for both doublet and quartet **TS1** show that the former reflects a more advanced TS by virtue of the significant elongation of the H^1 – C^3 bond and closer proximity of H^1 to the electrophilic nitrene. Conversely, for the ^4A state, the allylic hydrogen remains more closely associated with C^3 . The Ru^1 – N^5 bond in both depictions of **TS1** more closely approximates a single bond, and this change is matched with an

increased metal–metal interaction and a contracted $\text{Ru}^1\text{--Ru}^2$ bond length. The barrier heights, calculated as the energy difference between complex **6** and **TS1**, were found to be 14.8(16.7)[14.5] kcal/mol for doublet **TS1** and 6.8(11.2)[10.0] kcal/mol for quartet **TS1**.

The identification of a discrete diradical intermediate **7** (Figure 8) on the reaction coordinate for C–H amination with $[\text{Ru}_2(\text{hp})_4\text{Cl}]$ explains the penchant of this catalyst to effect allylic oxidation. The diradical species follows **TS1** as the result of H^1 -atom transfer to the metal-bound nitrogen. The computed electronic structure of **7** favors a ground-state quartet with three unpaired α -spins located primarily on the Ru^1 , Ru^2 , C^3 , and C^5 centers (see Table S1 in the SI). The doublet state of complex **7** is higher in energy by 7.8(12.7)[4.8] kcal/mol, with the unpaired spin distributed across the Ru^1 , Ru^2 , C^3 , and C^5 centers. The pathway to allylic amination thus begins with nitrenoid complex **6** in a doublet electronic ground state, proceeds through a 14.8(16.7)[14.5] kcal/mol energy barrier at the doublet state **TS1**, and leads to diradical intermediate **7** as a lowest-energy quartet. The doublet and quartet potential energy surfaces for the sequence $\mathbf{6} \rightarrow \mathbf{TS1} \rightarrow \mathbf{7}$ cross only after transition state **TS1**. Intermediate **7** is a local minimum on the potential energy surface (i.e., it has no imaginary frequencies) but is unstable both kinetically and thermodynamically and converges readily to the alkoxysulfonamide complex $\text{Ru}_2 \cdot \text{O}$ (see Figure 8).

All attempts to locate the TS associated with the conversion of diradical **7** to the complexed product $\text{Ru}_2 \cdot \text{O}$ failed. Scanning the potential energy surface of the reaction $\mathbf{7} \rightarrow \text{Ru}_2 \cdot \text{O}$ by fixing the reaction coordinate and the $\text{N}^5\text{--C}^3$ distance and then optimizing all other geometry parameters suggested a 0.5–0.8 kcal/mol energy barrier for the radical rebound step. This small kinetic barrier should require minimal structural reorganization for the biradical intermediate to pass through the associated transition state and on to $\text{Ru}_2 \cdot \text{O}$.

As depicted in Figure 8, the alkoxysulfonamide product (i.e., oxathiazinane) remains loosely associated with the diruthenium complex (as the adduct $\text{Ru}_2 \cdot \text{O}$) following C–N bond formation. The geometrical parameters for the diruthenium core of $\text{Ru}_2 \cdot \text{O}$ closely parallel those of the parent catalyst $[\text{Ru}_2(\text{hp})_4\text{Cl}]$; both the free complex and the oxathiazinane adduct have a quartet electronic ground state. Dissociation of the heterocycle from $\text{Ru}_2 \cdot \text{O}$ is calculated to be exothermic by 2.1(13.7)[9.8] kcal/mol.

In summary, the C–H insertion pathway beginning with doublet nitrenoid complex **6** proceeds through a 14.8(16.7)[14.5] kcal/mol energy barrier at transition state **TS1** (doublet), which leads to the quartet state diradical intermediate **7**. This process can be described as a severe C–H bond polarization from C^3 to the coordinated nitrene N^5 followed by homolytic bond scission and diradical formation. In the subsequent steps, radical recombination proceeds over an energy barrier of <1 kcal/mol to form the product-bound complex $\text{Ru}_2 \cdot \text{O}$. The overall conversion of the *trans*-4-hexenyl sulfamate nitrenoid to the oxathiazinane heterocycle via the sequence $\mathbf{6} \rightarrow \mathbf{TS1} \rightarrow \mathbf{7} \rightarrow \text{Ru}_2 \cdot \text{O}$ is calculated to be exothermic by 55.7(55.5)[51.8] kcal/mol.

Aziridination Pathway. The mechanism for alkene aziridination by $[\text{Ru}_2(\text{hp})_4\text{Cl}]$ was evaluated computationally in a manner analogous to that described for allylic oxidation. Three limiting transition structures for this process, which differ as a function of the angle of approach of the olefin moiety to the nitrene ligand, are depicted in Figure 9.

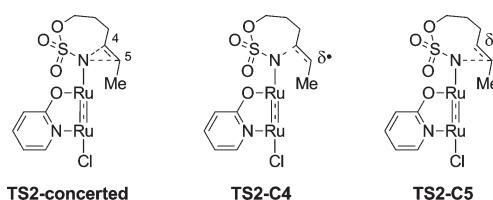


Figure 9. Possible transition structures for the alkene aziridination pathway. For clarity, only one of the four 2-oxypyridinate ligands in each structure is shown.

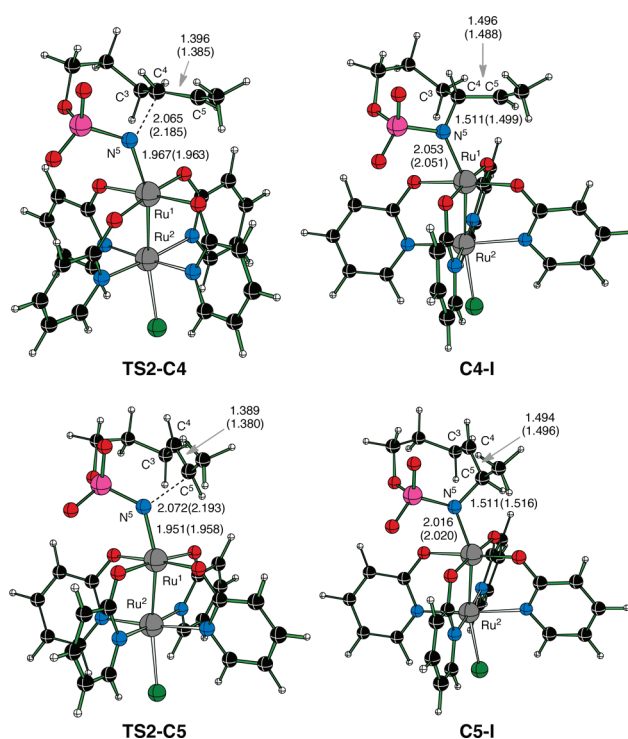


Figure 10. Computed structures of transition states **TS2-C4** and **TS2-C5** and their corresponding diradical intermediates **C4-I** and **C5-I** on the aziridination pathway. Numerical values represent bond lengths (in Å) for doublet electronic states. Corresponding values for quartet electronic states are in parentheses.

The calculations suggest the viability of either **TS2-C4** or **TS2-C5** but not the cyclic transition structure **TS2-concerted**, which represents a higher-energy pathway that converges to either **TS2-C4** or **TS2-C5**. Both **TS2-C4** and **TS2-C5** (Figure 10) are real and possess a single imaginary frequency, and both are ground-state doublets. The quartet transition states are higher in energy by 2.0(0.8)[0.8] kcal/mol for **TS2-C4** and 3.0(1.1)[1.1] kcal/mol for **TS2-C5**. Quasi-intrinsic reaction coordinate (quasi-IRC) calculations confirmed that **TS2-C4** and **TS2-C5** connect the nitrenoid complex **6** with intermediates **C4-I** and **C5-I**, respectively.

Close inspection of the calculated metrical parameters for **TS2-C4** reveals that along this pathway the $\text{Ru}^1\text{--N}^5$ and $\text{C}^4\text{--C}^5$ bond distances are elongated by 0.178 and ~ 0.06 Å, respectively, relative to those of the starting Ru –nitrene **6**. C^4 approaches N^5 at 2.065 Å (doublet) or 2.185 Å (quartet). Weakening of the $\text{Ru}^1\text{--N}^5$ bond in **TS2-C4** increases the $\text{Ru}^1\text{--Ru}^2$ bond strength and re-establishes its multibonding character. These structural

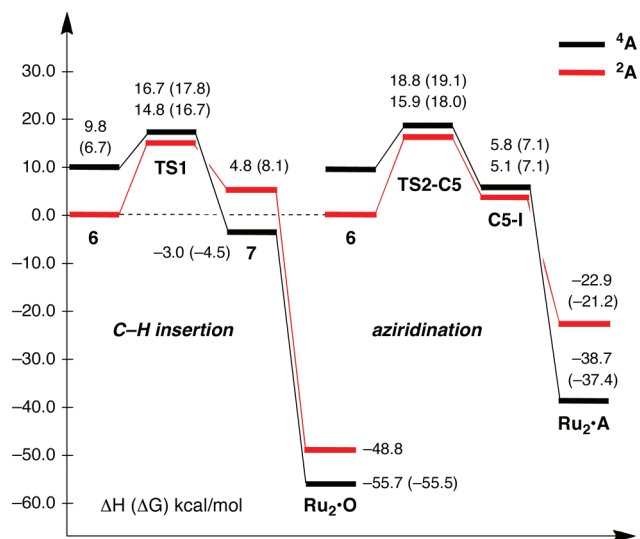


Figure 11. Relevant energies along the reaction coordinate for both allylic amine formation and aziridination (lowest-energy pathway via intermediate C5-I) computed for both doublet and quartet states.

modifications occur concomitantly with a spin density redistribution as the reaction progresses (see Table S1 in the Supporting Information).

Lengthening of the C⁴–C⁵ bond apportions 0.60 β -spin as a doublet or 0.53 α -spin as a quartet to the C⁵ center. In the doublet electronic state, the Ru¹ and N⁵ centers acquire 0.94 α -spin and 0.33 β -spin, respectively. The doublet electronic state of TS2-C4 differs from the quartet state essentially by a spin flip at the N⁵ and C⁵ centers. This finding is consistent with the small calculated energy difference of 2.0(0.8) kcal/mol between these two electronic states as well as the $\langle S^2 \rangle$ value of 1.58 for the doublet state. Surmounting the 19.1(21.4) kcal/mol energy barrier at TS2-C4 leads to the generation of intermediate C4-I with incipient N⁵–C⁴ bond formation at 1.511(1.499) Å (Figure 10), which weakens and stretches the Ru¹–N⁵ bond by 0.086(0.088) Å.

Formation of the N⁵–C⁵ bond follows via radical coupling to furnish the bicyclic aziridine, which remains loosely bound to the parent complex as [Ru₂(hp)₄Cl]·aziridine (Ru₂·A). Scanning the potential energy surface for the reaction pathway C4-I → Ru₂·A by fixing the reaction coordinate and the N⁵–C⁵ distance and then optimizing all other geometry parameters leads us to posit a 0.3–0.5 kcal/mol energy barrier from C4-I to Ru₂·A. Minimal structural reorganization is thus needed for C4-I to proceed to product; the relevant transition structure was not determined.

The alternative aziridination pathway, operating through initial approach of C⁵ to the N⁵ center, commences with metal-bound nitrene complex 6 and proceeds through transition state TS2-C5 (Figure 10). The calculated activation energy for aziridination of 6 via the lowest-energy doublet state of TS2-C5 was found to be 15.9(18.0)[20.6] kcal/mol. Quasi-IRC calculations confirmed that transition state TS2-C5 connects 6 with intermediate C5-I (Figure 10). Both the geometry and spin properties of C5-I exhibit a high degree of similarity to those of complex C4-I, except that spin density is transferred in this case to C⁴ rather than C⁵, which is the site of nascent bond formation. Intermediate C5-I converges to the metal-associated aziridine

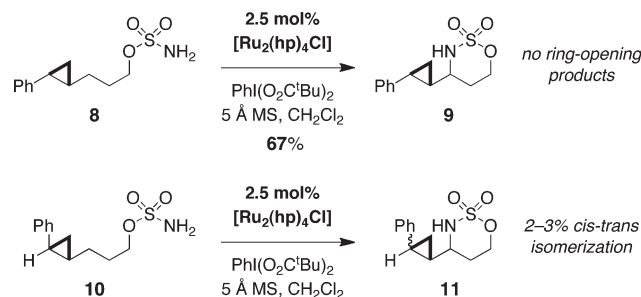
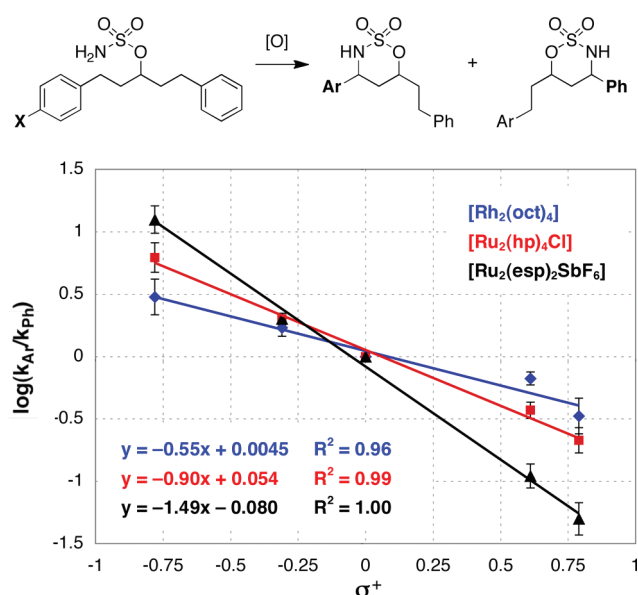


Figure 12. Partial cis–trans isomerization of 10 consistent with a short-lived radical intermediate.

complex Ru₂·A with a very small energy barrier; a transition state for this process could not be located. The aziridination process 6 → TS2-C5 → C5-I → Ru₂·A occurs exothermically by 38.7(37.4)[37.0] kcal/mol and in fact represents the lowest-energy operative mode for the aziridination process. Dissociation of the fused bicyclic heterocycle from complex Ru₂·A is exothermic by 5.6(16.8)[15.4] kcal/mol. The doublet and quartet potential energy surfaces of this reaction cross after intermediate C5-I en route to product.

Summary. As shown in Figure 11, the reaction coordinates for complementary amination pathways begin at the same doublet nitrenoid complex 6. The allylic pathway proceeds through a 14.8(16.7)[14.5] kcal/mol energy barrier at the doublet transition state TS1, characterized as a PCET TS, that leads through intermediate 7 to the heterocycle-bound complex Ru₂·O. The overall allylic C–H amination reaction leading to Ru₂·O is exothermic by 55.7(55.5)[51.8] kcal/mol. Alternatively, aziridination occurs through the favored doublet transition state TS2-C5 over a 15.9(18.0)[20.6] kcal/mol energy barrier and follows a pathway through intermediate C5-I that is downhill by 38.7(37.4)[38.0] kcal/mol. Thus, the energetic cost for C–H amination from nitrenoid 6 is 1.0(1.3)[6.1] kcal/mol less than that of the aziridination pathway. This calculated value is consistent with the 8:1 product selectivity noted in the reaction of 4-hexenyl sulfamate (see Table 1). Additionally, there is a clear thermodynamic preference (by 17.0(18.1)[14.8] kcal/mol) for six-membered-ring oxathiazinane formation through allylic C–H amination.

Mechanistic Analysis: Experimental. Experimental investigations were undertaken in an effort to substantiate the conclusions drawn from our DFT analysis. In order to distinguish a C–H abstraction/radical rebound mechanism, cyclopropane clock substrate 8 was subjected to amination conditions using 2.5 mol % [Ru₂(hp)₄Cl] (Figure 12). The rate constant for ring opening of a related cyclopropylcarbinyl radical has been estimated at $2 \times 10^{11} \text{ s}^{-1}$, which translates to a radical lifetime on the order of picoseconds.²⁹ Somewhat surprisingly, no fragmentation product was observed in the reaction of 8, and the six-membered oxathiazinane was obtained in 67% isolated yield. Because of the possible reversibility of cyclopropylcarbinyl radical ring fragmentation in 8, oxidation of the isomeric *cis*-cyclopropane substrate 10 was also conducted. In this case, HPLC analysis revealed that a small percentage (2–3%) of the *trans*-cyclopropane had indeed formed. This latter result is consistent with the intermediacy of a short-lived radical species that can reversibly fragment the adjacent ring before undergoing fast recombination.



X	σ^+	$[Rh_2(oct)_4]$ Ar/Ph	$[Ru_2(hp)_4Cl]$ Ar/Ph	$[Ru_2(esp)_2SbF_6]$ Ar/Ph
OMe	-0.78	3.0/1.0	6.2/1.0	12.5/1.0
Me	-0.31	1.7/1.0	2.0/1.0	2.0/1.0
CF ₃	0.61	1.0/1.5	1.0/2.7	1.0/9.1
NO ₂	0.79	1.0/3.0	1.0/4.7	1.0/20.0

Figure 13. Hammett analysis data for competitive intramolecular benzylic insertion using rhodium and ruthenium catalysts.

Insight into the transition structure of the oxidation event was obtained through Hammett analysis using a series of competitive sulfamate cyclization reactions on substrates possessing two electronically disparate benzylic centers (Figure 13). Values of ρ for reactions promoted by different metal complexes were determined by linear regression analysis of the logarithm of product ratios plotted against σ^+ . Analogous experiments with the dirhodium tetraoctanoate complex $[Rh_2(oct)_4]$, which likely operates through a concerted asynchronous reaction manifold, furnished a value of $\rho = -0.55$.^{25a} This small negative number reflects the stabilizing influence of electron-donating substituents and is consistent with a concerted transition state. By comparison, the ρ values for the two ruthenium catalysts $[Ru_2(hp)_4Cl]$ and $[Ru_2(esp)_2SbF_6]$ were determined to be -0.90 and -1.49 , respectively. Excellent fits to the data were obtained in all three cases, providing R^2 values near unity.

In comparison with $[Rh_2(oct)_4]$, the more negative ρ values for the two diruthenium complexes are indicative of transition structures in which C–H bond breakage is pronounced. In particular, $[Ru_2(esp)_2SbF_6]$, with a recorded ρ value of -1.49 , shows remarkable discrimination for the oxidation of electronically dissimilar C–H bonds (e.g., $[Ru_2(esp)_2SbF_6]$ furnishes a 20:1 ratio of insertion products favoring reaction at benzylic over *p*-nitrobenzylic centers). If one assumes that all three catalysts function through a concerted pathway, the evident differences in the Hammett data for the dirhodium- and diruthenium-catalyzed C–H aminations are not easily explained. The ostensibly most electrophilic catalyst, $[Ru_2(esp)_2SbF_6]$, which by inference should afford the most reactive nitrenoid, operates with the highest degree of chemoselectivity. An alternative interpretation of the data posits a change in mechanism from a concerted

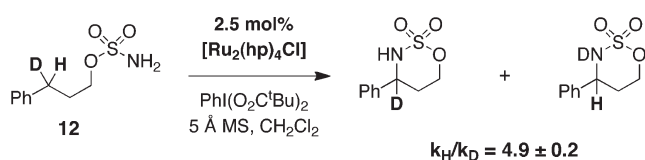


Figure 14. Deuterium-labeled sulfamate ester for KIE analysis.

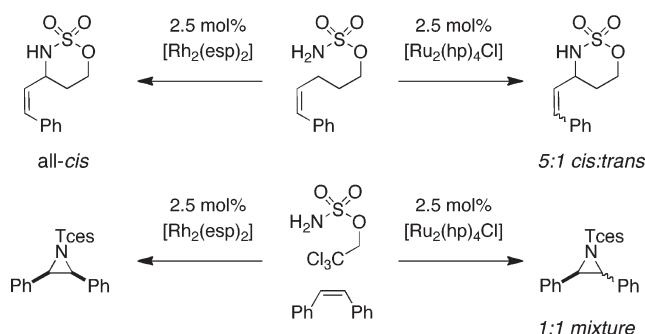


Figure 15. Comparison of reaction outcomes for Rh- and Ru-catalyzed amination reactions. All of the reactions were performed with 2.5 mol % catalyst and $PhI(O_2C^tBu)_2$ in CH_2Cl_2 . MgO and 5 Å molecular sieves were used as additives for reactions with the Rh and Ru catalysts, respectively (see the SI for details).

insertion process (rhodium) to one involving homolytic or heterolytic C–H bond cleavage (ruthenium). Such a stepwise process through a radical or cationic intermediate would account for the larger influence of substituent groups on the relative rates of C–H amination in the diruthenium-mediated reactions.

To probe further the mechanism of the diruthenium-catalyzed process, we measured the influence of deuterium substitution on the rate of C–H oxidation. A straightforward kinetic isotope effect (KIE) determination could be made by employing mono-deuterated starting material 12 (Figure 14). Under typical amination conditions with 2.5 mol % $[Ru_2(hp)_4Cl]$, the ratio of oxathiazinane isotopomers was determined to be 4.9 ± 0.2 (based on quantitative ^{13}C NMR analysis; see Supporting Information for details). This experimental value is in remarkably precise accord with the DFT-computed value of 4.9. By comparison, the experimentally measured KIE for the $[Rh_2(OAc)_4]$ -catalyzed reaction with 12 was 2.6 ± 0.2 .³⁰ These data strongly implicate a stepwise mechanism for C–H oxidation promoted by diruthenium catalysts. Such a pathway would be expected to favor nitrogen insertion into C–H bonds with lower homolytic bond strengths (i.e., allylic and benzylic).

Additional evidence in support of a $[Ru_2(hp)_4Cl]$ -mediated radical abstraction/rebound amination pathway follows from product analysis data. When subjected to the diruthenium-catalyzed amination process, one substrate, *cis*-5-phenyl-4-pentenyl sulfamate, yielded two isomeric products arising from partial scrambling of the double-bond geometry (Figure 15). The same reaction performed with $[Rh_2(esp)_2]$ gave exclusively the *cis* product. This observation offers compelling evidence for the intermediacy of a short-lived radical species en route to the product heterocycle.³¹ A similar set of experiments involving intermolecular aziridination of *cis*-stilbene further serves to highlight the stepwise nature of the diruthenium-catalyzed process. Taken together, these data offer definitive support for the stepwise mechanism for C–H and π -bond amination revealed by DFT.

CONCLUSIONS

We have demonstrated for the first time the efficacy of diruthenium complexes for catalytic oxidative amination of C–H bonds. The catalyst $[\text{Ru}_2(\text{hp})_4\text{Cl}]$ displays a preference for amination of allylic and benzylic centers, a characteristic that distinguishes its selectivity profile from dirhodium tetracarboxylate counterparts. Both computational and experimental data have revealed a mechanism for diruthenium-mediated C–H insertion that is stepwise in nature and progresses through the intermediacy of a short-lived diradical species. These conclusions contrast the apparent concerted, asynchronous mechanism for the dirhodium process and thus provide a rationale for the divergent trends in C–H bond chemoselectivity. The identification of $[\text{Ru}_2(\text{hp})_4\text{Cl}]$ as an effective agent for C–H amination opens the door to a new class of catalyst structures that can accommodate a wider range of ligand types than simple carboxylates. The discoveries detailed in this report therefore constitute an important step forward in the evolution of reagent-controlled methods for selective C–H bond oxidation.

ASSOCIATED CONTENT

S Supporting Information. General experimental protocols; characterization data for new compounds; complete ref 27a; calculated spin densities (in e) of important atoms of reactants, intermediates, transition states, and products of allylic amination and aziridination by complex **6** (Table S1); Cartesian coordinates (in Å) of all structures calculated at the B3LYP/LANL2DZ level of theory (Table S2); and crystallographic data (CIF). This material is available free of charge via the Internet at <http://pubs.acs.org>.

AUTHOR INFORMATION

Corresponding Author

dmusaev@emory.edu, jdubois@stanford.edu

ACKNOWLEDGMENT

Funding for this project was provided by the National Science Foundation Center for Stereoselective C–H Functionalization (CSCHF). D.G.M. acknowledges NSF Grant CHE-0553581 and the Cherry Emerson Center for Scientific Computation. We thank Dr. Allen Oliver at the University of Notre Dame for crystallographic analysis. We thank a reviewer for suggesting the experiment with *cis*-cyclopropane **10**.

REFERENCES

- (1) For recent reviews, see: (a) Davies, H. M. L.; Dick, A. R. *Top. Curr. Chem.* **2010**, 292, 303–346. (b) Doyle, M. P.; Duffy, R.; Ratnikov, M.; Zhoi, L. *Chem. Rev.* **2010**, 110, 704–724. (c) *Modern Rhodium-Catalyzed Organic Reactions*; Wiley-VCH: Weinheim, Germany, 2005; pp 301–340, 341–355, 357–377. (d) Davies, H. M. L.; Beckwith, R. E. J. *Chem. Rev.* **2003**, 103, 2861–2903.
- (2) Catino, A.; Forslund, R. E.; Doyle, M. P. *J. Am. Chem. Soc.* **2004**, 126, 13622–13623.
- (3) (a) Padwa, A.; Austin, D. J.; Hornbuckle, S. F.; Semones, M. A.; Doyle, M. P.; Protopopova, M. N. *J. Am. Chem. Soc.* **1992**, 114, 1874–1876. (b) Padwa, A.; Austin, D. J.; Price, A. T.; Semones, M. A.; Doyle, M. P.; Protopopova, M. N.; Winchester, W. R.; Tran, A. *J. Am. Chem. Soc.* **1993**, 115, 8669–8680.
- (4) For recent reviews of C–H amination, see: (a) Davies, H. M. L.; Manning, J. R. *Nature* **2008**, 451, 417–424. (b) Díaz-Requejo, M. M.; Pérez, P. J. *Chem. Rev.* **2008**, 108, 3379–3394. (c) Fantauzzi, S.; Caselli, A.; Gallo, E. *Dalton Trans.* **2009**, 5434–5443. (d) Collet, F.; Dodd, R. H.; Dauban, P. *Chem. Commun.* **2009**, 5061–5074. (e) Zalatan, D. N.; Du Bois, J. *Top. Curr. Chem.* **2010**, 292, 347–378. (f) Li, Z.; Capretto, D. A.; He, C. In *Silver in Organic Chemistry*; Harmata, M., Ed.; Wiley: Hoboken, NJ, 2010; pp 167–182. (g) Collet, F.; Lescot, C.; Dauban, P. *Chem. Soc. Rev.* **2011**, 40, 1926–1936.
- (5) For rhodium: (a) Espino, C. G.; Du Bois, J. *Angew. Chem., Int. Ed.* **2001**, 40, 598–600. (b) Espino, C. G.; Wehn, P. M.; Chow, J.; Du Bois, J. *J. Am. Chem. Soc.* **2001**, 123, 6935–6936. (c) Liang, J.-L.; Yuan, S.-X.; Chan, P. W. H.; Che, C.-M. *Org. Lett.* **2002**, 4, 4507–4510. (d) Wehn, P. M.; Lee, J.; Du Bois, J. *Org. Lett.* **2003**, 5, 4823–4826. (e) Fiori, K. W.; Fleming, J. J.; Du Bois, J. *Angew. Chem., Int. Ed.* **2004**, 43, 4349–4352. (f) Espino, C. G.; Fiori, K. W.; Kim, M.; Du Bois, J. *J. Am. Chem. Soc.* **2004**, 126, 15378–15379. (g) Kim, M.; Mulcahy, J. V.; Espino, C. G.; Du Bois, J. *Org. Lett.* **2006**, 8, 1073–1076. (h) Lebel, H.; Huard, K. *Org. Lett.* **2007**, 9, 639–642. (i) Stokes, B. J.; Dong, H.; Leslie, B. E.; Pumphrey, A. L.; Driver, T. G. *J. Am. Chem. Soc.* **2007**, 129, 7500–7501. (j) Fiori, K. W.; Du Bois, J. *J. Am. Chem. Soc.* **2007**, 129, 562–568. (k) Olson, D. E.; Du Bois, J. *J. Am. Chem. Soc.* **2008**, 130, 11248–11249. (l) Kurokawa, T.; Kim, M.; Du Bois, J. *Angew. Chem., Int. Ed.* **2009**, 48, 2777–2779. (m) Nörder, A.; Hermann, P.; Herdtweck, E.; Bach, T. *Org. Lett.* **2010**, 12, 3690–3692.
- (6) For copper: (a) Evans, D. A.; Faul, M. M.; Bilodeau, M. T. *J. Am. Chem. Soc.* **1994**, 116, 2742–2753. (b) Li, Z.; Conser, K. R.; Jacobsen, E. N. *J. Am. Chem. Soc.* **1993**, 115, 5326–5327. (c) Albane, D. P.; Aujla, P. S.; Taylor, P. J. *Org. Chem.* **1998**, 63, 9569–9571. (d) Brandt, P.; Södergren, M. J.; Andersson, P. G.; Norrby, P. O. *J. Am. Chem. Soc.* **2000**, 122, 8013–8020. (e) Badiei, Y. M.; Dinescu, A.; Dai, X.; Palomino, R. M.; Heinemann, F. W.; Cundari, T. R.; Warren, T. H. *Angew. Chem., Int. Ed.* **2008**, 47, 9961–9964. (f) Wiese, S.; Badiei, Y. M.; Gephart, R. T.; Mossin, S.; Varonka, M. S.; Melzer, M. M.; Meyer, K.; Cundari, T. R.; Warren, T. H. *Angew. Chem., Int. Ed.* **2010**, 49, 8850–8855. (g) Barman, D. N.; Liu, P.; Houk, K. N.; Nicholas, K. M. *Organometallics* **2010**, 29, 3404–3412.
- (7) For manganese and iron: (a) Breslow, R.; Gellman, S. H. *J. Chem. Soc., Chem. Commun.* **1982**, 1400–1401. (b) Breslow, R.; Gellman, S. H. *J. Am. Chem. Soc.* **1983**, 105, 6729–6730. (c) Mansuy, D.; Mahy, J. P.; Dureault, A.; Bedi, G.; Battioni, P. *J. Chem. Soc., Chem. Commun.* **1984**, 1161–1163. (d) Mahy, J. P.; Bedi, G.; Battioni, P.; Mansuy, D. *Tetrahedron Lett.* **1988**, 29, 1927–1929. (e) Yu, X.-Q.; Huang, J.-S.; Zhou, X.-G.; Che, C.-M. *Org. Lett.* **2000**, 2, 2233–2236. (f) Liang, J.-L.; Huang, J.-S.; Yu, X.-Q.; Zhu, N.; Che, C.-M. *Chem.—Eur. J.* **2002**, 8, 1563–1572. (g) Wang, Z.; Zhang, Y.; Fu, H.; Jiang, Y.; Zhao, Y. *Org. Lett.* **2008**, 10, 1863–1866. (h) King, E. R.; Betley, T. A. *Inorg. Chem.* **2009**, 48, 2361–2363.
- (8) For cobalt: (a) Ruppel, J. V.; Kamble, R. M.; Zhang, X. P. *Org. Lett.* **2007**, 9, 4889–4892. (b) Lu, H.; Jiang, H.; Wojtas, L.; Zhang, X. P. *Angew. Chem., Int. Ed.* **2010**, 49, 10192–10196. (c) Lu, H.; Tao, J.; Jones, J. E.; Wojtas, L.; Zhang, X. P. *Org. Lett.* **2010**, 12, 1248–1251.
- (9) For ruthenium: (a) Reference 7e. (b) Au, S. M.; Huang, J. S.; Che, C.-M.; Yu, W. Y. *J. Org. Chem.* **2000**, 65, 7858–7864. (c) Liang, J. L.; Yuan, S.-X.; Huang, J. S.; Che, C.-M. *J. Org. Chem.* **2004**, 69, 3610–3619. (d) Milczek, E.; Boudet, N.; Blakey, S. *Angew. Chem., Int. Ed.* **2008**, 47, 6825–6828.
- (10) For silver: (a) Cui, Y.; He, C. *Angew. Chem., Int. Ed.* **2004**, 43, 4210–4212. (b) Li, Z.; Rahaman, C. R.; He, C. *Angew. Chem., Int. Ed.* **2007**, 46, 5184–5186. (c) Gómez-Emeterio, B. P.; Urbano, J.; Díaz-Requejo, M. M.; Pérez, P. J. *Organometallics* **2008**, 27, 4126–4130.
- (11) For gold: (a) Li, Z.; Ding, X.; He, C. *J. Org. Chem.* **2006**, 71, 5876–5880. (b) Li, Z.; Capretto, D. A.; Rahaman, R. O.; He, C. *J. Am. Chem. Soc.* **2007**, 129, 12058–12059.
- (12) *Multiple Bonds Between Metal Atoms*, 3rd ed.; Cotton, F. A.; Murillo, C. A.; Walton, R. A., Eds.; Springer Science and Business Media: New York, 2005; pp 377–430.
- (13) (a) Barker, J. E.; Ren, T. *Inorg. Chem.* **2008**, 47, 2264–2266. (b) Murahashi, S.; Okano, Y.; Sato, H.; Nakae, T.; Komiya, N. *Synlett* **2007**, 1675–1678. (c) Komiya, N.; Nakae, T.; Sato, H.; Naota, T. *Chem. Commun.* **2006**, 4829–4831.

(14) (a) Pap, J. S.; DeBeer George, S.; Berry, J. F. *Angew. Chem., Int. Ed.* **2008**, *47*, 10102–10105. (b) Pap, J. S.; Snyder, J. L.; Piccoli, P. M. B.; Berry, J. F. *Inorg. Chem.* **2009**, *48*, 9846–9852. (c) Long, A. K. M.; Yu, R. P.; Timmer, G. H.; Berry, J. F. *J. Am. Chem. Soc.* **2010**, *132*, 12228–12230.

(15) $[\text{Rh}_2(\text{OAc})_4]$: $E_{1/2} = 1170$ mV vs SCE in CH_3CN . $[\text{Rh}_2(\text{HNC}(\text{OCH}_3)_4)_4]$: $E_{1/2} = 150$ mV vs SCE in CH_3CN . See: Zhu, T. P.; Ahsan, M. Q.; Malinski, T.; Kadish, K. M.; Bear, J. L. *Inorg. Chem.* **1984**, *23*, 2–3. $[\text{Ru}_2(\text{OAc})_4\text{Cl}]$: $E_{1/2} > 1600$ mV vs SCE in CH_3CN . See: Cotton, F. A.; Pederson, E. *Inorg. Chem.* **1975**, *14*, 388–391. $[\text{Ru}_2(\text{HNC}(\text{OCH}_3)_4\text{Cl})]$: $E_{1/2} = 470$ mV vs SCE in DMSO. See: Chavan, M. Y.; Feldmann, F. N.; Lin, X. Q.; Bear, J. L.; Kadish, K. M. *Inorg. Chem.* **1984**, *23*, 2373–2375.

(16) For a general review of allylic amine synthesis, see: Jørgensen, K. A. *Modern Allylic Amination Methods*. In *Modern Amination Methods*; Ricci, A., Ed.; Wiley-VCH: Weinheim, Germany, 2007.

(17) (a) Fraunhofer, K. J.; White, M. C. *J. Am. Chem. Soc.* **2007**, *129*, 7274–7276. (b) Liu, G.; Yin, G.; Wu, L. *Angew. Chem., Int. Ed.* **2008**, *47*, 4733–4736. (c) Reed, S. A.; White, M. C. *J. Am. Chem. Soc.* **2008**, *130*, 3316–3318. (d) Rice, G. T.; White, M. C. *J. Am. Chem. Soc.* **2009**, *131*, 11707–11711. (e) Reed, S. A.; Mazzotti, A. R.; White, M. C. *J. Am. Chem. Soc.* **2009**, *131*, 11701–11706. (f) Yin, G.; Wu, Y.; Liu, G. *J. Am. Chem. Soc.* **2010**, *132*, 11978–11987.

(18) Zalatan, D. N.; Du Bois, J. J. *Am. Chem. Soc.* **2008**, *130*, 9220–9221.

(19) (a) Liang, C.; Collet, F.; Robert-Peillard, F.; Müller, P.; Dodd, R. H.; Dauban, P. J. *Am. Chem. Soc.* **2008**, *130*, 343–350. (b) Collet, F.; Lescot, C.; Liang, C.; Dauban, P. *Dalton Trans.* **2010**, *39*, 10401–10413.

(20) Stephenson, T. A.; Wilkinson, G. J. *Inorg. Nucl. Chem.* **1966**, *28*, 2285–2291.

(21) Chakravarty, A. R.; Cotton, F. A.; Tocher, D. A. *Inorg. Chem.* **1985**, *24*, 172–177.

(22) Selective allylic amination, albeit in modest yield, can be performed with a dirhodium tetracarboxamidate catalyst (see ref 18). For examples of Ru–pybox-catalyzed intramolecular allylic amination of sulfamate esters, see ref 9d.

(23) For a discussion of diastereoselectivity in C–H functionalization reactions, see: Herrmann, P.; Bach, T. *Chem. Soc. Rev.* **2011**, *40*, 2022–2038.

(24) Wehn, P. M.; Lee, J.; Du Bois, J. *Org. Lett.* **2003**, *5*, 4823–4826.

(25) (a) Fiori, K. W.; Espino, C. G.; Brodsky, B. H.; Du Bois, J. *Tetrahedron* **2009**, *65*, 3042–3051. (b) Lin, X.; Zhao, C.; Che, C.-M.; Ke, Z.; Phillips, D. L. *Chem.—Asian J.* **2007**, *2*, 1101–1108. (c) Huard, K.; Lebel, H. *Chem.—Eur. J.* **2008**, *14*, 6222–6230. (d) Nägeli, I.; Baud, C.; Bernardinelli, G.; Jacquier, Y.; Moran, M.; Müller, P. *Helv. Chim. Acta* **1997**, *80*, 1087–1105.

(26) (a) Au, S. M.; Huang, J. S.; Yu, W. Y.; Fung, W. H.; Che, C.-M. *J. Am. Chem. Soc.* **1999**, *121*, 9120–9132. (b) Leung, S. K. Y.; Tsui, W. M.; Huang, J. S.; Che, C.-M.; Liang, J. L.; Zhu, N. *J. Am. Chem. Soc.* **2005**, *127*, 16629–16640.

(27) All calculations were performed using the Gaussian 09 quantum-chemical program package [(a) Frisch, M. J.; et al. *Gaussian 09*, revision B.01; Gaussian, Inc.: Wallingford, CT, 2010]. The geometries of all species under investigation were optimized without symmetry constraints at the B3LYP level of theory [see: (b) Becke, A. D. *Phys. Rev. A* **1988**, *38*, 3098–3107. (c) Lee, C.; Yang, W.; Parr, R. G. *Phys. Rev. B* **1988**, *37*, 785–789. (d) Becke, A. D. *J. Chem. Phys.* **1993**, *98*, 1372–1380.] in conjunction with LANL2DZ basis sets and the corresponding Hay–Wadt effective core potentials (ECPs) for Ru centers and 6-31G(d) split-valence basis sets for other atoms [see: (e) Hay, P. J.; Wadt, W. R. *J. Chem. Phys.* **1985**, *82*, 270–283. (f) Hay, P. J.; Wadt, W. R. *J. Chem. Phys.* **1985**, *82*, 299–310. (g) Wadt, W. R.; Hay, P. J. *J. Chem. Phys.* **1985**, *82*, 284–298.]. This method is subsequently called “B3LYP/LANL2DZ”. Hessian matrices were calculated for all species under investigation. All reported transition states were confirmed to have a single imaginary frequency corresponding to the reaction coordinate. Quasi-IRC calculations were utilized for further elucidation of the nature these transition states. The solvent effects were estimated at

the B3LYP/LANL2DZ level of theory using the polarizable continuum model (PCM) method [see: (h) Cancès, E.; Mennucci, B.; Tomasi, J. *J. Chem. Phys.* **1997**, *107*, 3032–3041.] at the gas-phase optimized geometries. In these calculations, CH_2Cl_2 was used as the solvent.

(28) Similar findings have been reported for electron-deficient nitrenes. See: (a) Gritsan, N. P.; Platz, M. S.; Borden, W. T. *Mol. Supramol. Photochem.* **2005**, *13*, 235–236. (b) Liu, J.; Hadad, C. M.; Platz, M. S. *Org. Lett.* **2005**, *7*, 549–552.

(29) Valentine, A. M.; LeTadic-Biadatti, M. H.; Toy, P. H.; Newcomb, M.; Lippard, S. J. *J. Biol. Chem.* **1999**, *274*, 10771–10776.

(30) In prior work (see ref 25a), we reported a KIE of 1.9 ± 0.2 for the $\text{Rh}_2(\text{OAc})_4$ -catalyzed oxidation of sulfamate **12**. This value was obtained using ^{13}C NMR spectroscopy following a protocol outlined by Wang and Adams to measure the KIE for intramolecular Rh–carbene C–H insertion (see: Wang, P.; Adams, J. *J. Am. Chem. Soc.* **1994**, *116*, 3296–3305). For the present study, all KIE measurements were made using a 90 s relaxation delay to ensure accurate signal integration. For the $\text{Rh}_2(\text{OAc})_4$ reaction, a slightly higher KIE value of 2.6 ± 0.2 was recorded when these alternative acquisition parameters were used.

(31) We appreciate that there is an apparent discrepancy between the results shown in Figure 15 and the calculated diradical rebound barrier of 0.5–0.8 kcal/mol for *trans*-4-hexenyl sulfamate. At this time, we can only surmise that our calculations underestimate this energy value or that the barrier for the rebound event is substrate-dependent. Additional studies to understand the origin of these differences are in progress.